

Sunspot Oscillations and Acoustic Wave Propagation

P.Brekke¹, N. Brynildsen², P. Maltby², T. Fredvik², and O. Kjeldseth-Moe²

¹European Space Agency, NASA Goddard Space Flight Center, Maryland 20771, USA

²Institute of Theoretical Astrophysics, University of Oslo, Oslo, Norway

Abstract

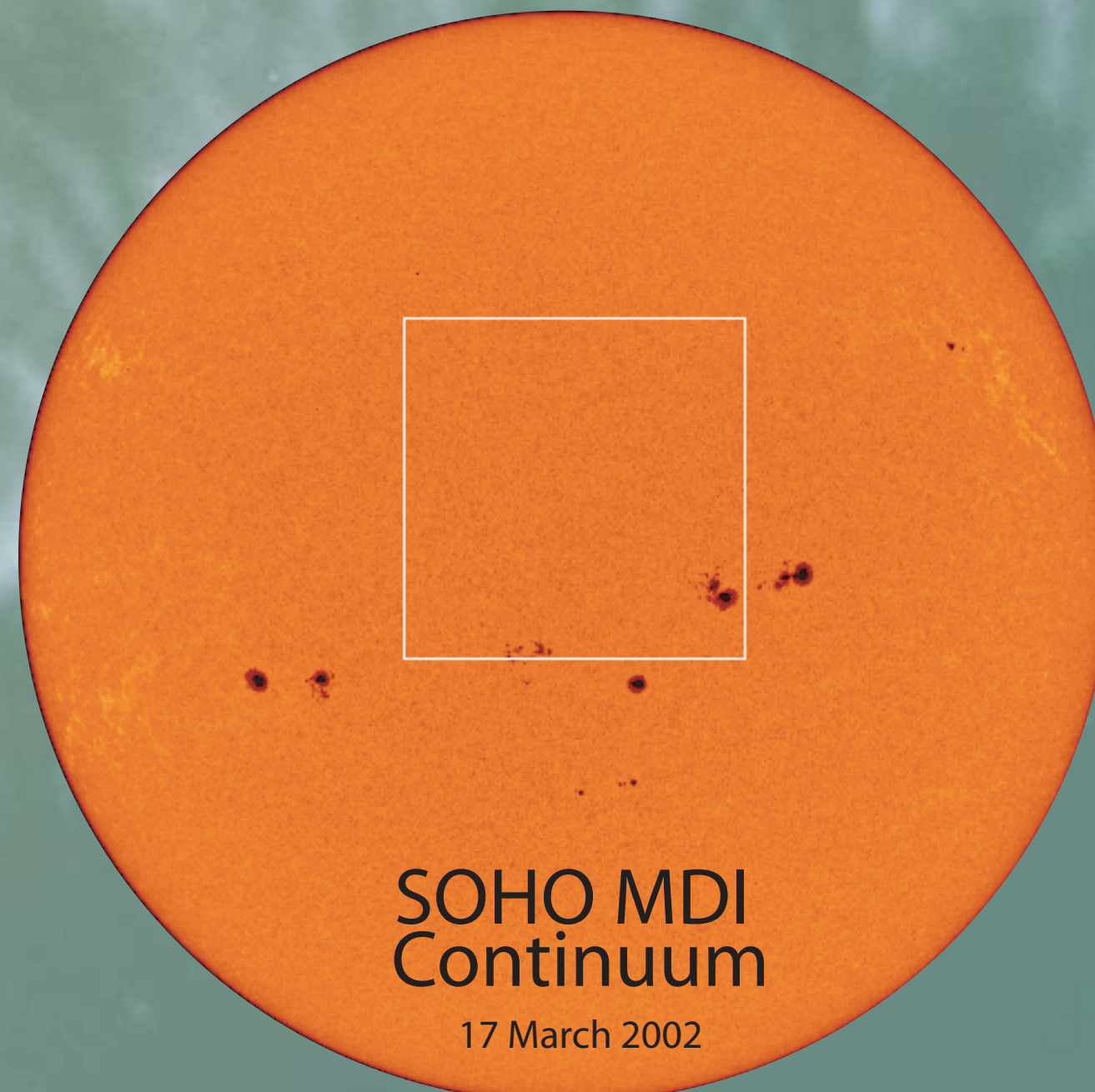
Observations with the Coronal Diagnostic Spectrometer of 3 min oscillations in sunspot umbrae support the hypothesis that they are caused by upwardly propagating acoustic waves. This is evident from the asymmetry of oscillation amplitudes in the red and blue wings of spectral lines, where the oscillations are decidedly more pronounced in the blue than in the red line wing. Additional evidence include the fact that the relation between oscillations in intensity and velocity agree with that predicted for an acoustic wave with regard to phase as well as magnitude. Finally, the observed phase difference between lines formed at different temperatures points to an upward propagating disturbance, and the value of dominant frequency of the oscillations, close to 6 mHz, is above the acoustic cutoff frequency in the sunspot atmosphere.

Simple Wave

Consider a one-dimensional traveling, nonlinear acoustic wave without shocks, often called a simple wave. For a polytropic gas the relation between the particle velocity, u , and the density, ρ , is (e.g., Landau and Lifshitz, 1987):

$$\frac{\rho}{\rho_0} = \left[1 \pm \frac{1}{2} (\gamma - 1) \frac{u}{c_0} \right]^{2/(\gamma - 1)} \quad (1)$$

The index 0 denotes an undisturbed value, γ is the polytropic index and C_0 is the sound speed. Since we measure velocities away from the observer as positive, the minus sign should be selected for a wave propagating towards the observer. To a first approximation the line intensity, I , of optically thin emission lines is proportional to ρ^2 (e.g., Mariska 1992). Hence, we may calculate the line profile for an emission line, formed in a region where a nonlinear acoustic wave propagates towards the observer with, say, $\Delta I/I = (\Delta \rho/\rho_0)^2 = 0.25$. For $\gamma = 5/3$ and $C_0 = 69 \text{ km s}^{-1}$ the calculated O V $\lambda 629$ line profile is shown in Figure 5 for three instances of time corresponding to the phase, ϕ , being equal to $0, \pi/2$, and $3\pi/2$.



Observations

As a part of our ongoing sunspot program in August 2001 and March 2002 we observed nine different sunspot regions with CDS. The CDS programme involves both the Normal Incidence Spectrometer - NIS and the Grazing Incidence Spectrometer - GIS.

The programme starts and ends by NIS rastering an area of $120'' \times 120''$ with a $2'' \times 240''$ slit. The GIS $4'' \times 4''$ slit is positioned in the leading part of the sunspot, allowing the solar rotation to move the sunspot image over the slit while consecutive spectra are recorded. GIS records the oscillations in emission lines in four wavelength bands, 151-221, 256-338, 393-493, and 656-785 Å. The programme then moves to NIS, letting the solar rotation move the sunspot image over the $2'' \times 240''$ slit while consecutive spectra in six wavelength regions are observed.

Results

The present CDS observations show 3 min oscillations above each umbra and the corresponding power spectra show one dominant frequency close to 6 mHz.

The observations support the hypothesis that the 3 min oscillations are caused by upwardly propagating acoustic waves since:

- (1) the dominant frequency, close to 6 mHz, see Figure 1 and 2, is above the acoustic cutoff frequency in the sunspot atmosphere (e.g., Shibasaki, 2001).
- (2) the phase difference between the observed lines is compatible with an upwardly propagating wave, see Figure 2.
- (3) the amplitudes of the oscillations in the blue wing are considerably larger than the amplitudes in the red wing, see Figure 4 and compare with the calculations in Figure 5.
- (4) the relations between the oscillations in intensity and line-of-sight velocity agree with those predicted for an acoustic wave, both regarding the phase and the magnitude, see Figure 3 and 6.

SOHO is a mission of international cooperation between ESA and NASA. This study was supported by the Research Council of Norway.

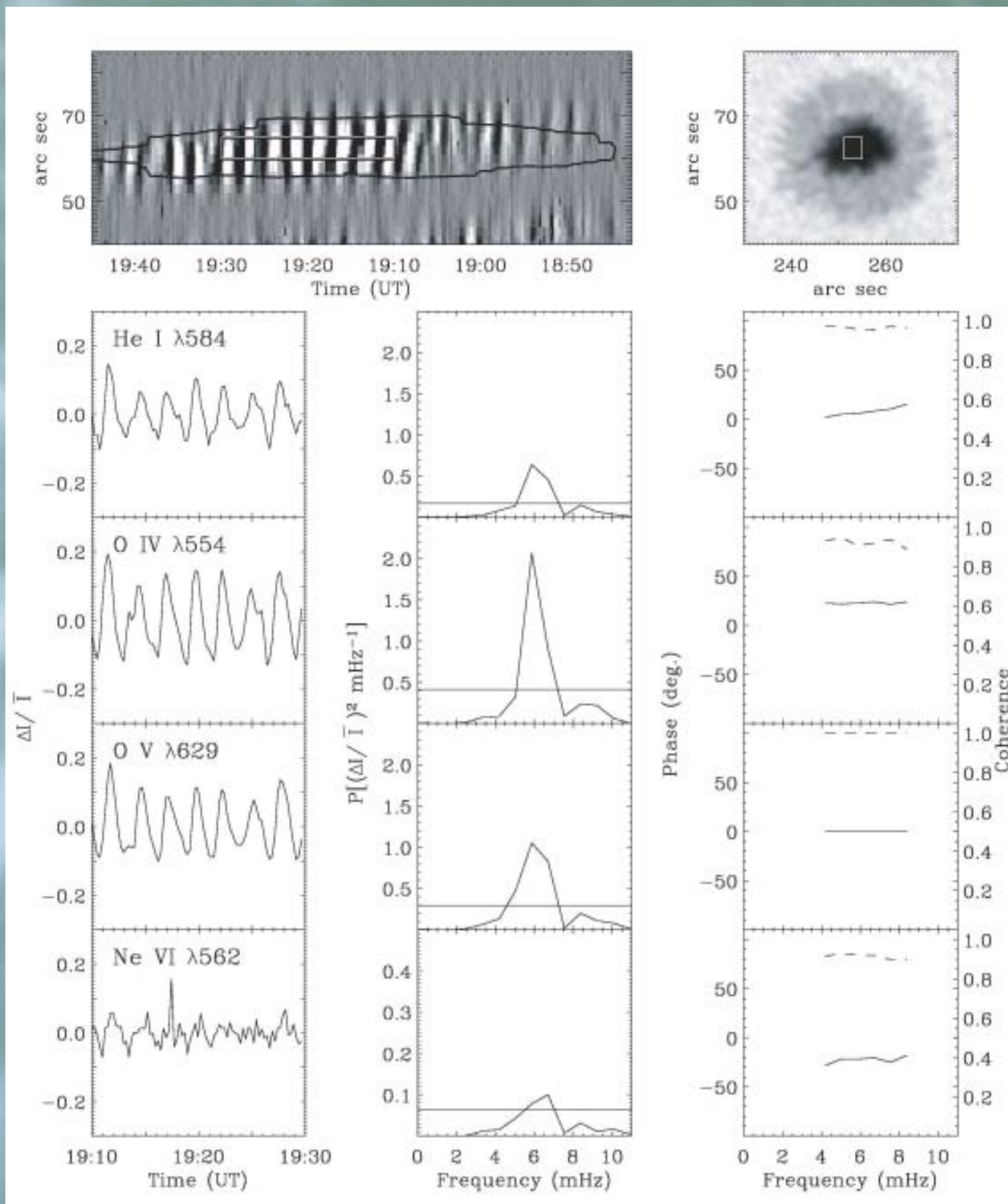


FIGURE 1: The relative integrated line intensity, $\Delta I/I$, along the NIS slit in the O IV 554 line in NOAA 9575 as a function of time on 18 August 2001 (top, left). The umbra rim is shown in the O IV $\lambda 554$ recordings and corresponding areas are marked with white rectangles in O IV $\lambda 554$ and the white-light image (top, right). The scales in arc sec are in a reference system where the origin coincides with the centre of the solar disk. Left to right: Oscillations in $\Delta I/I$ in the marked area above the umbra, followed by the corresponding power spectra, $P[(\Delta I/I)^2]$, and the phase and coherence (dashed) relative to the O V $\lambda 629$ line. Note that the Ne VI $\lambda 562$ power spectrum is plotted on a different scale. The horizontal lines mark three times the noise level in the power spectra plots. The plots are ordered with line formation temperature increasing from top to bottom.

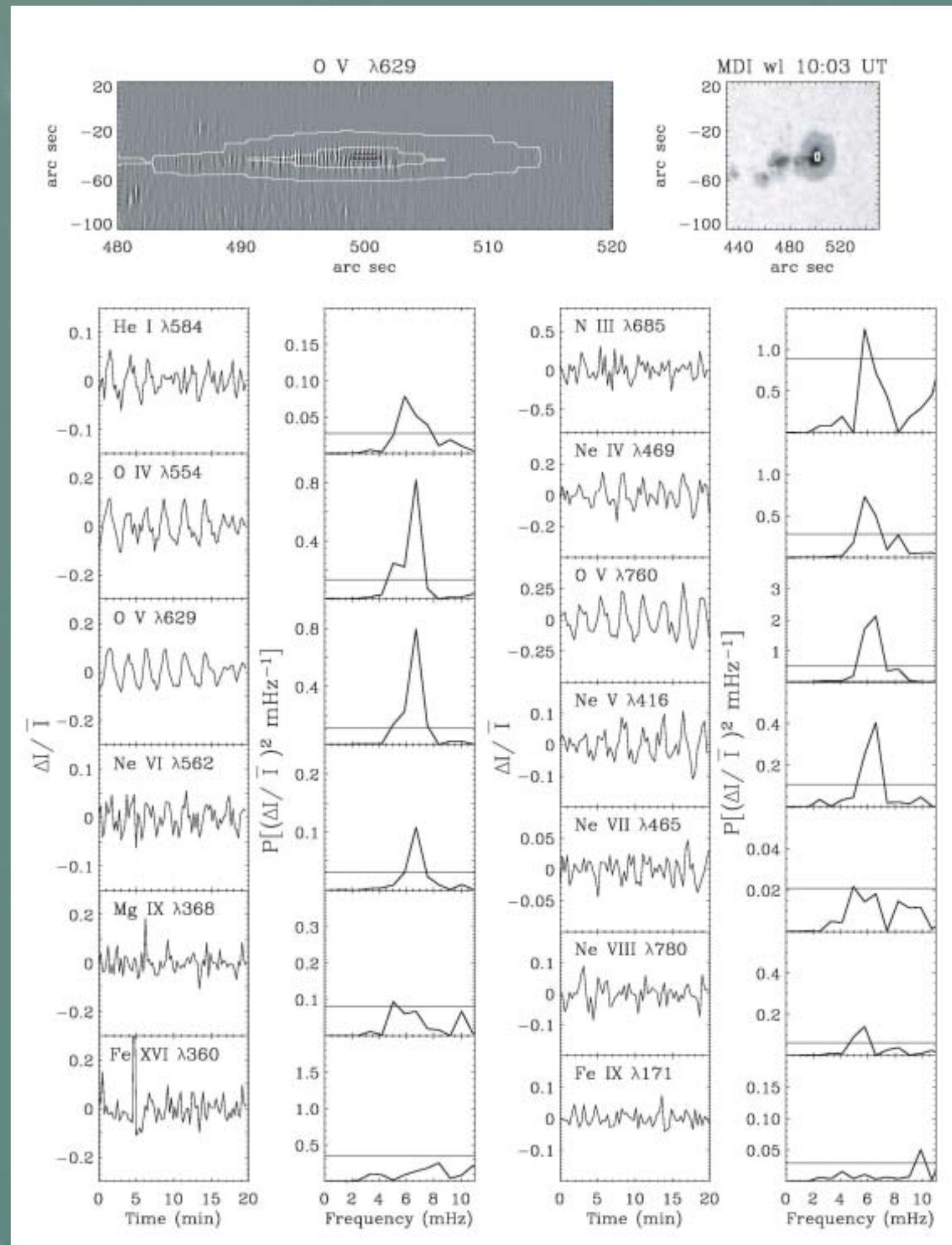


FIGURE 2: The relative integrated line intensity, $\Delta I/I$, along the NIS slit in O V $\lambda 629$ as a function of time for the leading sunspot in NOAA 9866 on 17 March 2002 (top, left). The umbra and penumbral contours are marked in the O V $\lambda 629$ recordings and corresponding rectangles are marked with white contours in O V $\lambda 629$ and in the umbra of the white-light image (top, right). Left to right: Temporal variation in $\Delta I/I$ within the marked rectangle observed with NIS, followed by the corresponding power spectra, $P[(\Delta I/I)^2]$, next $\Delta I/I$, recorded with GIS and the corresponding power spectra, $P[(\Delta I/I)^2]$. The horizontal lines in the power spectra plots mark three times the noise level. Note that the scales may differ. The plots are ordered with line formation temperature increasing from top to bottom.

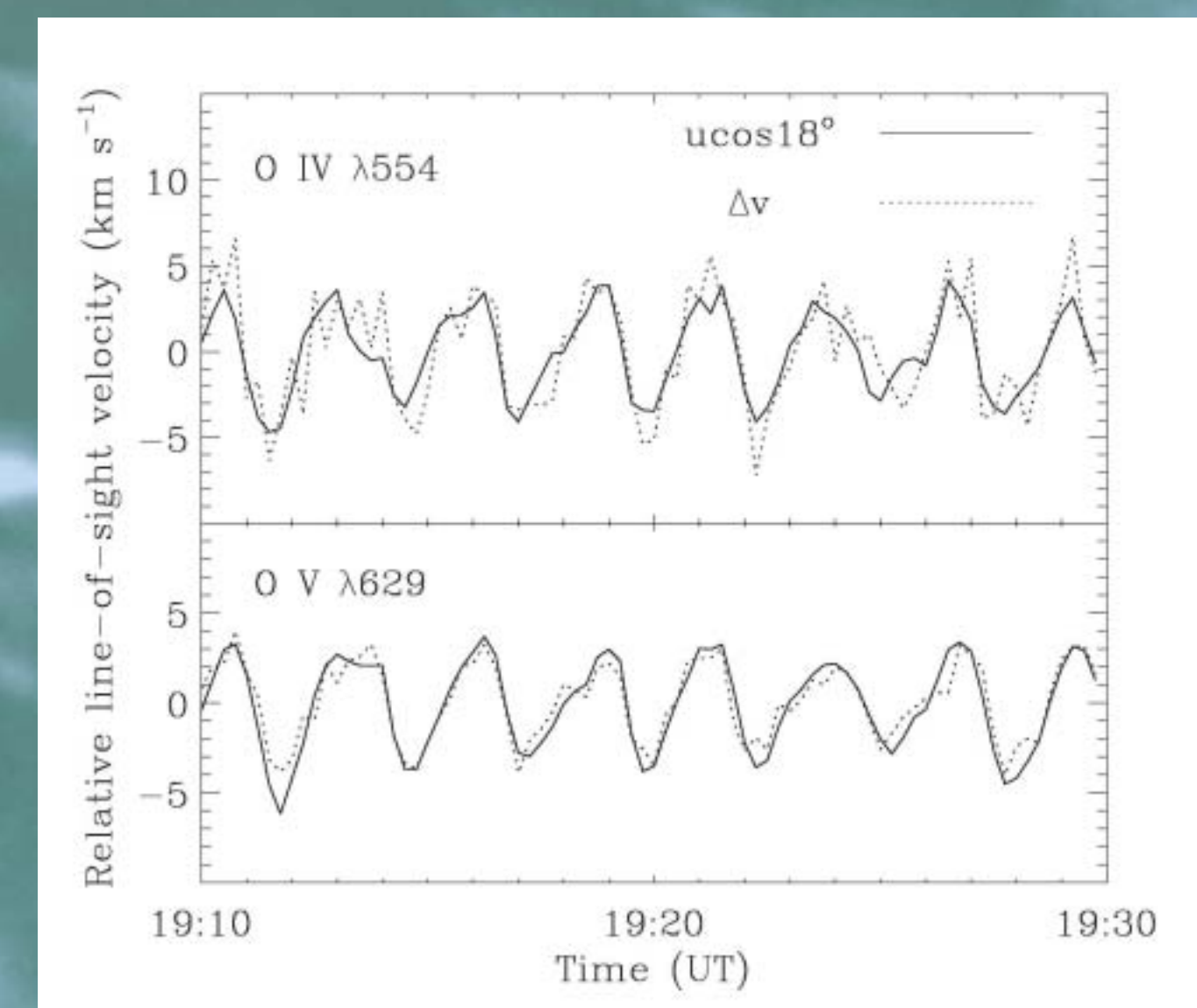


FIGURE 3: Temporal variation in calculated (Simple wave) line-of-sight velocity, $u \cos 18^\circ$ (solid line) and the observed line-of-sight velocity, Δv , (dotted) for NOAA 9575 observed on 18 August 2001.

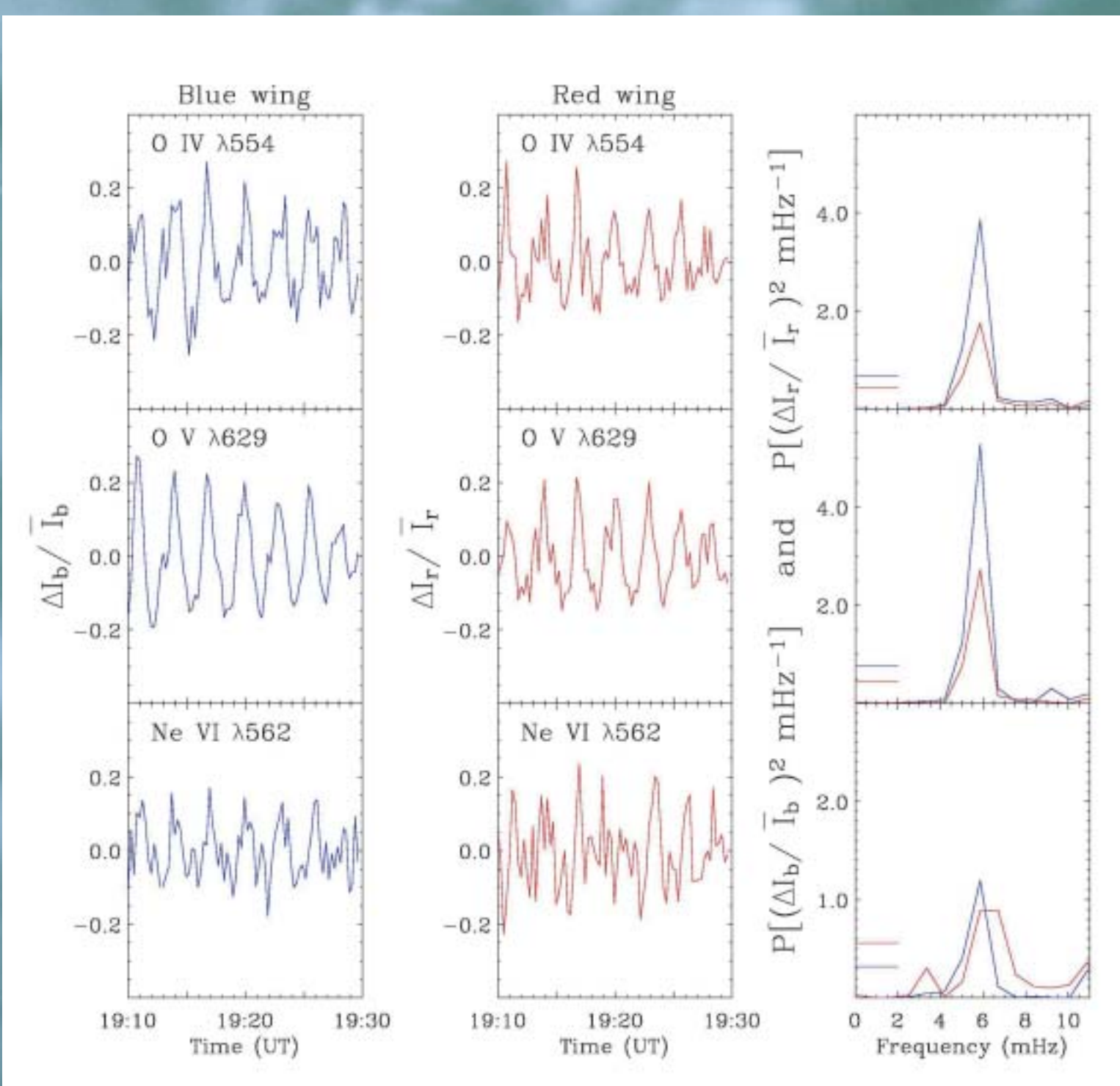


FIGURE 4: Left to right: The temporal variation in relative line intensity in the blue wing, $\Delta I_b/I_b$, followed by the temporal variation in the red wing, $\Delta I_r/I_r$, and the corresponding power spectra, $P[(\Delta I_b/I_b)^2]$ and $P[(\Delta I_r/I_r)^2]$, for lines observed on 12 March 2002 in NOAA 9866. The horizontal bars in the power plots mark three times the noise level.

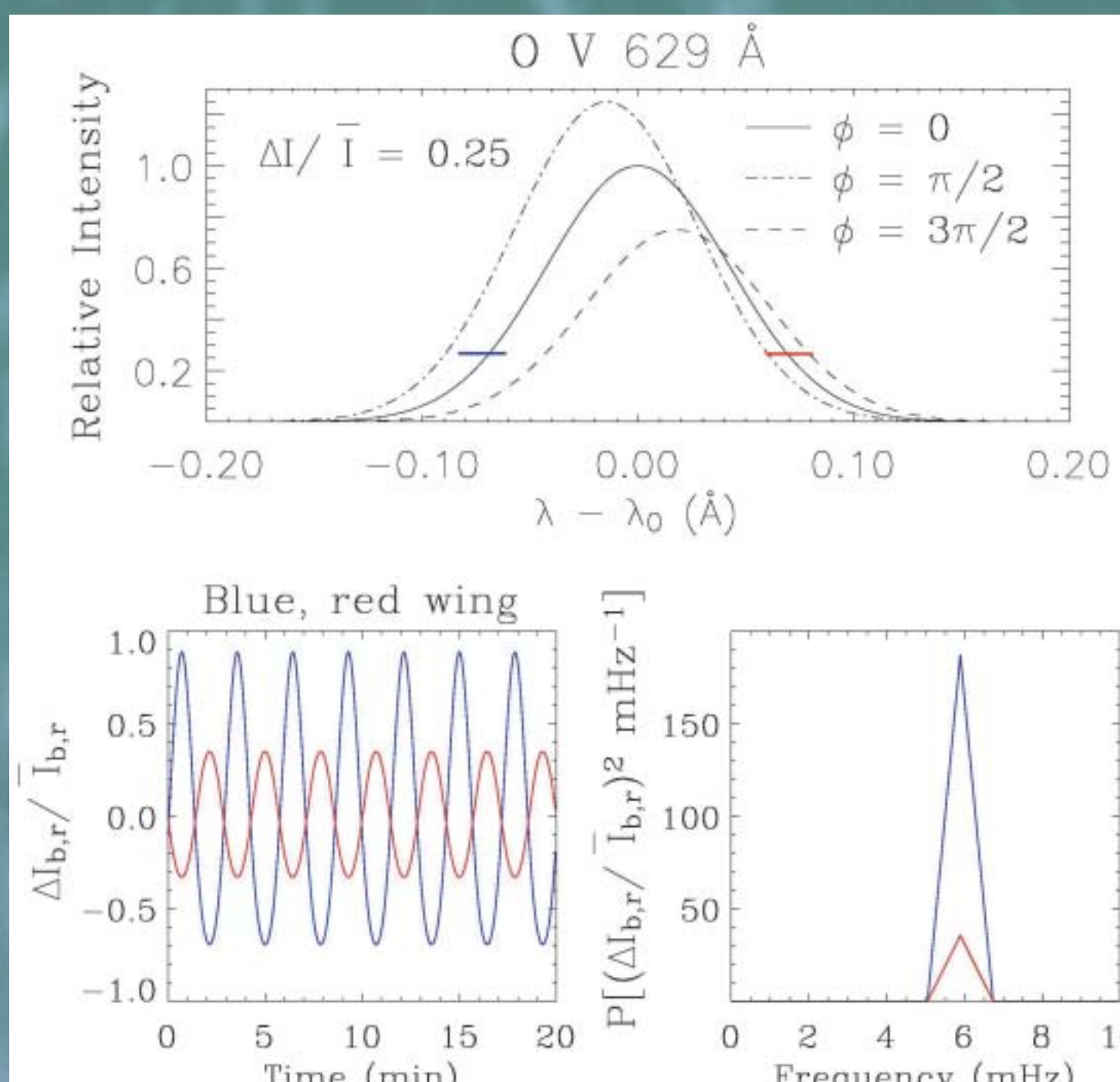


FIGURE 5: Calculated O V $\lambda 629$ line profiles, emitting from a region pervaded by an upwardly propagating, nonlinear acoustic wave with $\Delta I/I = (\Delta \rho/\rho_0)^2 = 0.25$ for three values of the phase $\phi = 0, \pi/2$ and $3\pi/2$. The locations of the blue and red wings are marked with horizontal bars. The calculated temporal variations in relative line intensity in the blue $\Delta I_b/I_b$ and the red wing $\Delta I_r/I_r$, and the corresponding power spectra, $P[(\Delta I_b/I_b)^2]$ and $P[(\Delta I_r/I_r)^2]$, are shown in the bottom diagrams.

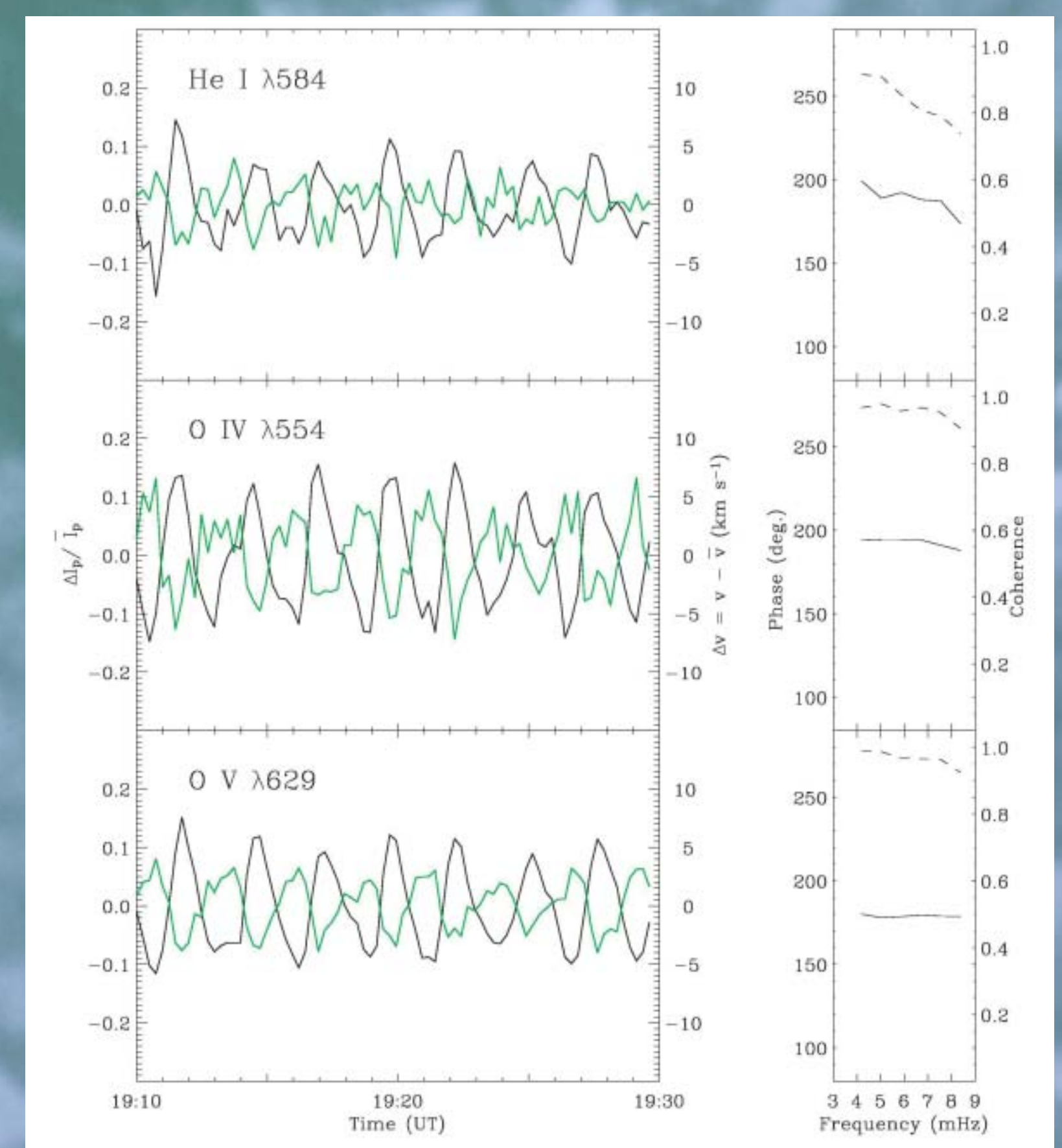


FIGURE 6: From left to right: The temporal variations in relative peak line intensity, $\Delta I_p/I_p$ (black line) and relative line-of-sight velocity, Δv (green line), followed by the corresponding coherence (dashed) and the phase difference between the line-of-sight velocity and the peak line intensity for lines observed with CDS/NIS on 18 August 2001 in NOAA 9575.